Track formation in SiO$_2$ quartz and the thermal-spike mechanism

A. Meftah
*Centre Interdisciplinaire de Recherches avec les Ions Lourds,
Boîte Postale 5133, 14040 Caen Cedex, France*

F. Brisard and J. M. Costantini
Commissariat á l' Energie Atomique, Service PTN, Boîte Postale 12, 91680 Bruyères-le-Châtel, France

E. Dooryhee
*Centre Interdisciplinaire de Recherches avec les Ions Lourds,
Boîte Postale 5133, 14040 Caen Cedex, France*

M. Hage-Ali
Centre de Recherches Nucléaires, Groupe Phase, 67037 Strasbourg Cedex, France

M. Hervieu
CRISMAT, Institut des Sciences de la Matière et du Rayonnement, Boulevard du Maréchal Juin, 14050 Caen Cedex, France

J. P. Stoquert
Centre de Recherches Nucléaires, Group Phase, 67037 Strasbourg Cedex, France

F. Studer
CRISMAT, Institut des Sciences de la Matière et du Rayonnement, Boulevard du Maréchal Juin, 14050 Caen Cedex, France

M. Toulemonde
*Centre Interdisciplinaire de Recherches avec les Ions Lourds,
Boîte Postale 5133, 14040 Caen Cedex, France*

α-quartz has been irradiated with heavy ions: ^{19}F, ^{32}S, and ^{63}Cu at an energy of about 1 MeV/amu in order to cover a range of electronic stopping powers dE/dx between 2.4 and 9 keV/nm and ^{58}Ni, ^{86}Kr, ^{128}Te, ^{129}Xe, ^{181}Ta, and ^{208}Pb between 1 and 5.8 MeV/amu for $dE/dx > 7$ keV/nm. The extent of the induced damage is determined using Rutherford backscattering ion channeling with a 2-MeV ^{4}He beam. The damage cross section A is obtained using a Poisson law $F_d = 1 - \exp(-A\phi t)$, where ϕ is the flux and t the irradiation time. This damage cross section is linked to the effective radius R_e through the relation $A = \pi R_e^2$, where R_e is the radius of an equivalent cylinder of damage. Using high-resolution electron microscopy, cylinders of amorphous matter have been observed, whose radius corresponds to R_e when the track is continuous (i.e., for $A \geq 1.3 \times 10^{-13}$ cm^2; $R_e \geq 2$ nm). A thermal-spike model is applied to calculate the radii of the observed tracks assuming that the observed amorphous cylinders correspond to a rapid quench of a molten liquid phase along the ion path. The model is applied only when the latent track is continuous and cylindrical. A good agreement is obtained taking into account that the initial spatial energy deposition on the electrons depends on the ion velocity.

I. INTRODUCTION

In most insulators a strongly damaged zone is induced along the ion path by the slowing down of a swift heavy ion. Although much work has been done over the past 30 years[1-6] in order to describe the latent tracks, the damage mechanism is still unclear. Several authors have proposed different models in order to explain these mechanisms. For insulators resistant to radiolysis one may think of the thermal spike,[7] the ionic spike[1] (where atomic motion is induced by the electrostatic repulsion of close neighbor ionized atoms) or more refined models.[3,8] For example, the role of target inner-shell electron excita-

tions was invoked, as a source of local intense ionizations, which trigger the damage formation process.[9] However it has been shown experimentally[10] that it is not necessary to invoke the inner-shell electron excitation as the major cause of the damage formation process. If the ionic-spike model was proposed to account for the track formation,[1] Sigrist and Balzer[11] have shown later on that the electronic stopping power threshold as deduced from the chemical etching of several insulators cannot be scaled by the parameters governing the ionic spike. On the contrary a better correlation appears between this threshold and the thermal conductivity of these insulators. In the same way, the electronic sputtering[12,13] was

also interpreted on the basis of a thermal process. Hence it appears that the thermal spike could be the predominant mechanism of the induced damage.

An other argument is in favor of the thermal spike: In the past the ionic-spike model has been developed to take into account the nonoccurrence of latent tracks in metallic materials. On the contrary, numerous recent experiments have shown that the electronic stopping power is efficient to create damage in crystalline metals,[14-16] in amorphous metallic and semiconductor materials.[17-20] From all these results it appears that materials with a strong electron-phonon coupling such as amorphous metallic alloys, or crystalline Ti and Fe,[15] and materials with a low value of melting point such as Bi,[16] are sensitive to intense electronic excitations. These observations are in favor of the thermal-spike model which describes the relaxation of the deposited energy through the electron-electron and the electron-phonon interactions. The thermal-spike model[21,22] was developed further and could explain quantitatively the damage creation in amorphous materials[21] and in pure metals.[16] In insulators, electrons can readily interact with the polar and acoustic modes of the lattice vibrations indicating a strong electron-phonon interaction. Based on this property of the insulators, the thermal-spike model was previously developed to account qualitatively for the latent tracks.[7,23,24] Hence it is now proposed to consider the conclusions of Sigrist and Balzer[11] in the framework of the thermal-spike model.[21] For this purpose SiO_2 quartz has been chosen in order to quantify experimentally the damage induced by swift heavy ions. In SiO_2 quartz all the physical and structural properties are well known in both its crystalline and amorphous phases. α-quartz (crystalline SiO_2) is known to be sensitive to high electronic excitations.[1,10,25,26] But there are only some scarce data[10] on the damage cross section evolution after swift heavy-ion irradiations. Therefore a systematic study of the damage creation in SiO_2 quartz has been undertaken over a wide range of the electronic stopping power (1.6 keV/nm $< dE/dx <$ 27.8 keV/nm). The radii of the latent tracks have been measured using Rutherford backscattering ion channeling (RBS-C) and electron microscopy. Furthermore the thermal-spike model is applied to calculate the radii of the observed latent tracks assuming that the observed disordered cylinders result from a rapid quench of a molten liquid phase.

II. EXPERIMENTAL CONDITIONS AND DAMAGE ANALYSIS

Slabs of synthetic optical quality, α-quartz single crystals, were purchased from "Quartz et Silice." They were 1.5 mm thick and covered with a 50-nm carbon layer in order to avoid electrostatic charging during irradiation or analysis.

Several different irradiations were performed at room temperature at the 7-MV tandem Van de Graaff at Bruyères le Châtel and at the Grand Accélérateur National d'Ions Lourds (GANIL) accelerator in Caen using the medium energy line facility.[27] The different experimental conditions are the following for the Van de Graaff
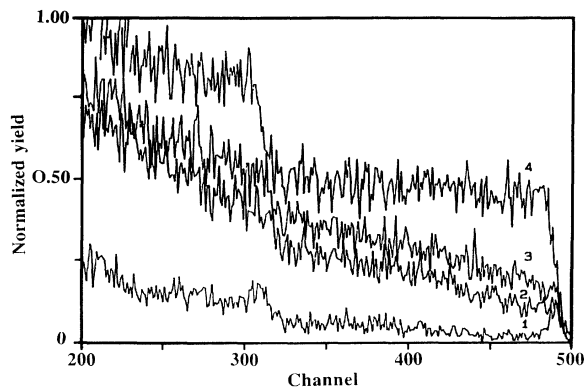

FIG. 1. Energy spectra of backscattered ^{4}He on α-quartz. Curve 1: $\langle 0001 \rangle$ virgin sample in channeling conditions. Curves 2 and 3: 11 MeV ^{63}Cu irradiated quartz, at 1.4×10^{12} and 2.8×10^{12} cm^{-2}, respectively. Curve 4: Virgin sample randomly oriented.

accelerator: ^{19}F, ^{32}S, and ^{63}Cu beams were used at incident energies of 0.79, 1.56, and 0.79 meV/amu, respectively, in order to cover a range of dE/dx between 2.4 and 9 keV/nm. Degradors before the samples were used to get different values of dE/dx with the same ion beam. For the GANIL accelerator, the beams were ^{58}Ni, ^{86}Kr, ^{128}Te, ^{129}Xe, ^{181}Ta, and ^{208}Pb at incident energies of 5.8, 3.4, 2.1, 1.5, 1.1, and 5.0 MeV/amu with $dE/dx > 7$ keV/nm, also by using a degrader when possible. The dE/dx values were calculated using the TRIM 91 code.[28] The beam flux was of the order of 10^9 ions/s/cm^2 at the tandem Van de Graaff and 3×10^8 ions/s/cm^2 at the GANIL accelerator. The maximum fluences range between 10^{11} and 10^{14} ions/cm^2 depending on the induced damage yield.

For the analysis of the radiation damage, Rutherford backscattering ion channeling (RBS-C) was performed on all the samples at the 4-MV Van de Graaff accelerator at the Centre de Recherches Nucléaires in Strasbourg. Figure 1 shows some RBS-C spectra of irradiated and nonir-
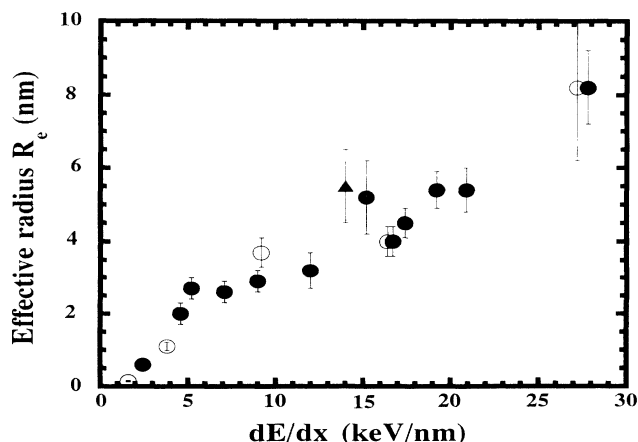

FIG. 2. The effective radius $R_e = \sqrt[2]{A/\pi}$ vs the electronic stopping power dE/dx. A is the damage cross section. ●: present work, ○: (Ref. 9), ▲: electron microscopy (present work).

TABLE I. Experimental data. A, R_e, and R_d are the damage cross section, the effective radius of the latent track, and the radius cylinder in which 65% of dE/dx is deposited, respectively.

Sample number	Ion	Energy [MeV/amu]	R_d (Ref. 32) [nm]	dE/dx [keV/nm]	A [cm²]	R_e [nm]	Reference
1	^{16}O	1.88	4.2	1.61	$(7.5\pm1.5)10^{-16}$	0.15+0.02	9
2	^{19}F	0.79	2.9	2.44	$(1.1\pm0.3)10^{-14}$	0.6±0.1	Present work
3	^{35}Cl	4.29	5.7	3.82	$(4.0\pm0.8)10^{-14}$	1.1±0.1	9
4	^{32}S	1.56	3.8	4.6	$(1.2\pm0.3)10^{-13}$	2.0±0.3	Present work
5	^{63}Cu	0.17	1.5	5.2	$(2.2\pm0.4)10^{-13}$	2.7±0.3	Present work
6	^{58}Ni	5.82	6.5	7.1	$(2.1\pm0.4)10^{-13}$	2.6±0.3	Present work
7	^{63}Cu	0.79	2.8	9.0	$(2.6\pm0.5)10^{-13}$	2.9±0.3	Present work
8	^{58}Ni	1.9	4.2	9.2	$(4.2\pm0.9)10^{-13}$	3.7±0.4	9
9	^{86}Kr	3.4	5.2	12.0	$(3.3\pm1.0)10^{-13}$	3.2±0.5	Present work
10	^{128}Te	2.1	4.3	15.2	$(8.5\pm2.5)10^{-13}$	5.2±0.8	Present work
11	^{127}I	1.48	3.7	16.4	$(5.0\pm1.0)10^{-13}$	4.0±0.4	9
12	^{129}Xe	1.5	3.7	16.7	$(5.0\pm1.0)10^{-13}$	4.0±0.4	Present work
13	^{128}Te	1.2	3.5	17.4	$(6.3\pm1.0)10^{-13}$	4.5±0.4	Present work
14	^{181}Ta	1.1	3.3	19.2	$(9.1\pm1.6)10^{-13}$	5.4±0.5	Present work
15	^{208}Pb	1.0	3.2	20.9	$(9.3\pm2.1)10^{-13}$	5.4±0.6	Present work
16	^{238}U	15.2	9.5	27.2	$(2.1\pm1.0)10^{-12}$	8.2±2.0	9
17	^{208}Pb	5.0	6.2	27.8	$(2.1\pm0.5)10^{-12}$	8.2±1.0	Present work
18	^{208}Pb [Micr.]	0.3	1.9	14.0		5.5±1.0	Present work

radiated SiO₂ quartz in channeling conditions along the $\langle 0001 \rangle$ direction. Using the surface approximation, the backscattering yield χ was measured by extrapolating the energy evolution of χ over the first 500-nm up to the mean energy of the random edge. The evolution of the fraction of damaged material F_d can be calculated $(\chi_i - \chi_v)/(\chi_r - \chi_v)$, where χ_i, χ_v, χ_r are the backscattering yields of the irradiated sample and of the virgin sample in channeling conditions and in random orientation, respectively. The damage cross section A was extracted using a Poisson law $F_d = 1 - \exp(-A\phi t)$, where ϕ is the flux and t the irradiation time. The damage cross sections A deduced from Ref. 10 and from this work are given in Table I. The effective radius R_e (Ref. 6) is deduced from the damage cross section $A = \pi R_e^2$ and is plotted versus dE/dx (Fig. 2). R_e corresponds to the radius of an equivalent cylinder in which the disordered phase is concentrated.

III. ELECTRON MICROSCOPY

A sample irradiated by lead ions was examined by electron microscopy. The nonirradiated face of a single crystalline slab has been chemically thinned in a fluorhydric acid solution down to 80 μm thickness. The slab was then thinned down on both faces by an argon beam in a Tech Ltd. ion-milling system leaving a hole in the center of the slab. The edges of the hole in the middle of the thickness at 40 μm from both faces were observed. This part of the sample corresponds approximately to a beam energy of the order of 0.3 MeV/amu ($dE/dx = 14$ keV/nm).

The bright-field images (Fig. 3), obtained from a JEOL 200 CX transmission electron microscope, show a distribution of almost circular and regular areas exhibiting a white contrast with regard to the surrounding dark ma-

trix. The number of white dots (1.2×10^{11} holes/cm²) is quite in agreement with the fluence (1.4×10^{11} Pb/cm²) suggesting that they correspond to the latent tracks. The high-resolution electron microscopy (HREM) study was performed with a TOPCON 002B electron microscope having a point resolution of 0.18 nm. The HREM image (Fig. 4) corresponds to the projected electron density image of the $\langle 0001 \rangle$ crystallographic plane of α-quartz. The inset (Fig. 4) shows the amorphous character of the latent track core in the crystalline matrix. From such an image, the radius of the amorphous cylinder can be easily measured: $R = (5.5 \pm 1.0)$ nm. This radius is in agreement with the effective radius deduced from the RBS-C experiments (see Table I; $R_e = 5.2$ nm at $dE/dx = 15.2$ KeV/nm). This result is also in agreement with the previous observation.[6,29] The typical long and cylindrical
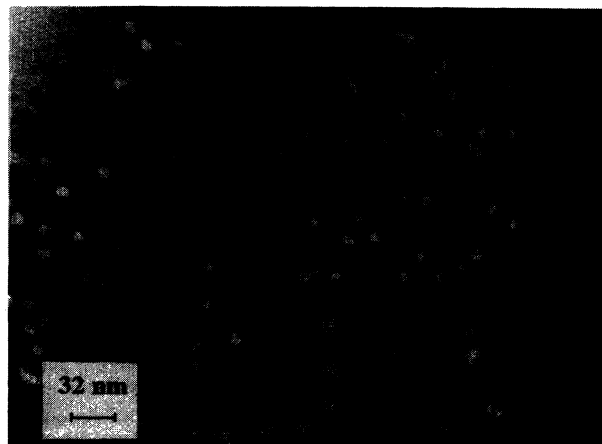

FIG. 3. Medium resolution electron microscopy observation of SiO₂ quartz irradiated by Pb ions ($E = 0.3$ MeV/amu; $\phi t = 1.4 \times 10^{11}$ ions/cm²).
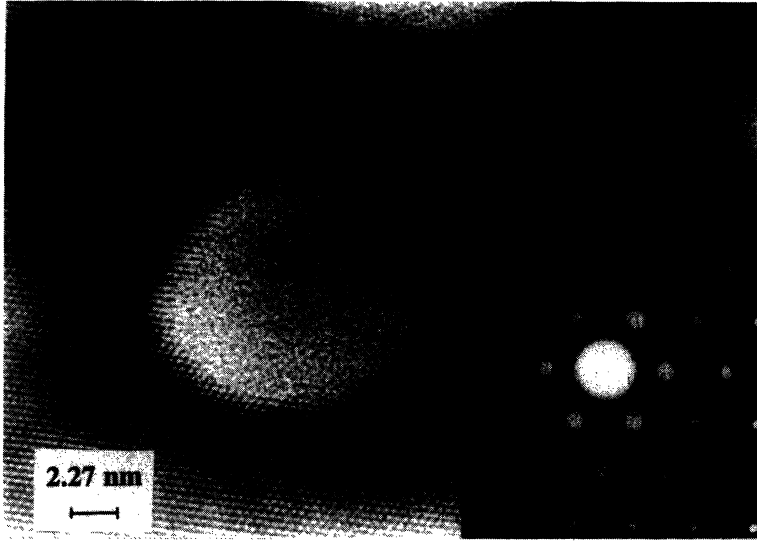
FIG. 4. High-resolution electron micrograph of an amorphized fragment of SiO_2 irradiated by Pb ions (0.3 MeV/amu). The electron diffraction in the inset shows typical diffuse rings indicating the presence of the amorphous phase.

shape of the latent tracks appears only $R_e \geq 2$ nm (or $A \geq 1.3 \times 10^{-13}$ cm^2), (as observed by HREM, $R_e = R$).

Under the electron beam of the microscope used for the observation, the image appears stable during a few minutes. Then as observed by Pascucci, Hutchinson, and Hobbs[30] the latent track radius starts to increase inducing a progressive and complete amorphization of the matrix. The phenomenon occurs sooner when increasing the electron beam flux.

IV. THE EFFECT OF THE ION VELOCITY ON THE DAMAGE YIELD

Recently[31] it has been shown that the damage cross section in yttrium iron garnet $Y_3Fe_5O_{12}$ is higher at low ion velocity than at high ion velocity for the same value of dE/dx. Katz and Kobetich[32] have calculated the spatial energy distribution of the energy deposited on the electrons: This distribution is broader at high velocity

than at low velocity. That is to say that for the same value of dE/dx the local deposited energy per unit volume is larger at low velocity than at high velocity. Waligorski, Hamm, and Katz[33] have proposed an analytical formula to describe the radial profile of the spatial energy deposition deduced from a fit of Monte Carlo results. Using this formula, the fraction of deposited energy in a cylinder of radius R_d is calculated and reported in Fig. 5 for different values of the incident energy. As it was defined for $Y_3Fe_5O_{12}$,[31] the R_d value (Table I) is the radius of a cylinder which absorbs 65% of the incident energy. For each value of dE/dx, the energy density D_e is defined as

$$D_e = \frac{0.65(dE/dx)}{N_a \pi R d^2},$$

where N_a is the atomic density. The effective radius R_e is plotted versus D_e in Fig. 6. A guide line links the
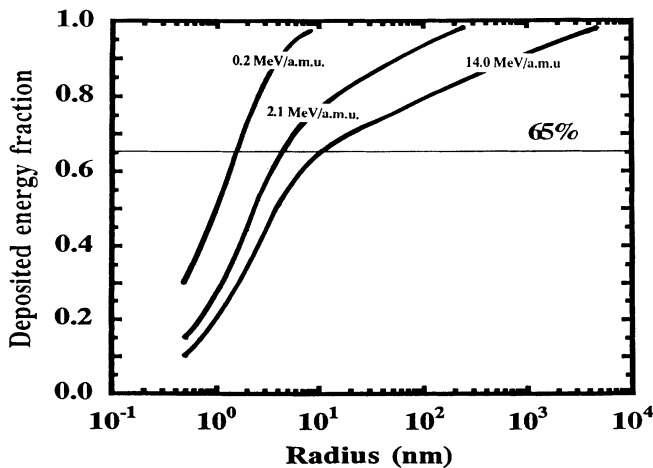

FIG. 5. The fraction of the deposited energy in a cylinder of radius R vs R, deduced from the calculation from Waligorski, Hamm, and Katz (Ref. 32). The incident ion energies are quoted on the curves.
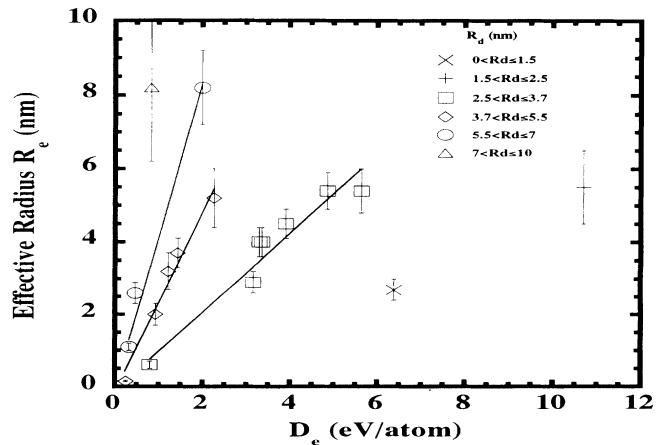

FIG. 6. The effective radius R_e vs the energy density D_e deposited in the core of the track. The lines are only to guide the eyes and link the R_e values corresponding to a specific range of R_d, where R_d is the radius of the cylinder in which 65% of dE/dx is deposited.

different values of R_e corresponding to a specific range of R_d. When the same energy density is deposited in a larger cylinder, the effective radius R_e (or the damage cross section) is larger. Knowing R_d and D_e, such a description (Fig. 6) enables one to predict the amount of ion-transformed quartz for any projectile at any velocity. Values of R_e in yttrium garnet can also be plotted out as a function of D_e (Ref. 31) and one can now explain all the previous results in Y₃Fe₅O₁₂.

V. CALCULATION OF THE LATENT TRACK RADII: THE THERMAL-SPIKE MODEL

The thermal-spike model was used[21] in order to calculate the radii of the latent tracks in amorphous semiconductors and metallic materials assuming that the latent tracks result from a rapid quenching of a liquid phase. In the same way, it is assumed that amorphous SiO₂ results from a quench of liquid SiO₂. This result is based on the fact that the observed phase transformation induced by heavy-ion irradiation may result from an increase of the lattice temperature through a two step process: thermalization of the electrons via electron-electron interaction and transfer of the deposited energy to the lattice via the electron-atom interactions. An analytical solution of this process is given by two coupled equations,[21,22,34] which describe the energy diffusion and the energy exchange over the electronic and over the atomic subsystems, respectively.

The mechanism of heat transfer from the electrons to the lattice depends on whether the material is a metal or an insulator. In metals, the heat conduction due to free electrons essentially results in the replacement of hot electrons inside the excited region by cold electrons from the periphery of the region. In insulators, the charges are immobile and there are no free electrons outside the excited region. Therefore Baranov *et al.*[12] proposed the following description: Hot electrons in the conduction band behave like in metals. The energy dissipation in the electronic system proceeds via bound electrons, when hot electrons ionize atoms at the periphery of the excited region. The energy spread ceases when the electron temperature becomes less than the optical band gap. But the parameters describing the energy relaxation on the electron subsystem and the energy transfer to the atoms cannot be determined as in a metal.[34,35] Hence we shall only use a simplified model of the thermal spike[21] which supposes that all the parameters describing the thermal evolution of the excited electron system are constant. In this model the main parameter is the mean free path of the electron λ. The electron scattering taking into account the electron-electron and electron-atom interactions are included in λ.[21] $\lambda = \sqrt{D\tau}$ where D is the thermal electron diffusivity of the hot electrons[12] and τ the electron-atom relaxation time. This parameter λ is the only free parameter which is linked to the confinement of the energy deposited on the electrons by the optical band gap.[12] Then the equation describing the energy diffusion equation on the electrons can be analytically solved. This gives the amount $N(r,t)$ of energy exchanged with the atoms. Then only the heat diffusion on the atoms is nu-

merically solved. In that case the atomic temperature is given by

$$\rho C(T)\frac{\partial T}{\partial t} = \frac{\partial}{\partial r}(K(T))\frac{\partial T}{\partial r} + \frac{K(T)}{r}\frac{\partial T}{\partial r} + N(r,t) \,,$$

where ρ, $C(T)$, $K(T)$, T, r, and t are the mass density, the specific heat, the thermal conductivity, the temperature, the radial distance, and the time, respectively. The energy deposition is given by $N(r,t)$ in cylindrical coordinates:[21,34]

$$N(r,t) = \frac{dE}{dx}\frac{1}{\tau}\exp\left[-\frac{t}{\tau}\right]\frac{1}{4\pi\sigma^2}\exp\left[-\frac{r^2}{4\sigma^2}\right] \,,$$

where

$$\sigma^2 = \frac{R_d^2}{4} + D \cdot t \,.$$

The thermal diffusivity of the excited electrons is independent of temperature and equal to 2 cm²/s.[35,36] It corresponds to a mean free path of one interatomic distance[36] for an electron excited in the conduction band. Two values of D and τ leading to the same value of λ will give the same result for the calculation, if D ranges between 1 and 10 cm²/s.

Since all the parameters in the energy diffusion equation on the atoms are temperature dependent (Table II), only a numerical solution has been performed taking also into account the solid→liquid phase transition when the temperature exceeds the melting temperature. In such a calculation, the temperature evolution[21] is followed versus time in successive rings of matter around the ion path. The purpose is to determine the radius of the cylinder of molten matter and then to compare it with R_e. The cylinder of amorphous phase of radius R_e is assumed to result from the quench of the liquid phase. The calculation does not take into account the thermal behavior of amorphous SiO₂ during the quenching stage, since the maximum radius of the molten phase is reached during the heating of the crystal material. It is known that the shape of the latent track is not always cylindrical (Refs. 4, 6, 31, 37, and 38). From the work performed on Y₃Fe₅O₁₂, a direct correlation appears between the ex-

TABLE II. Macroscopic thermodynamical parameters for SiO₂ quartz.

Thermal conductivity (Watt/K cm)	Solid	$T > 100$ K
		$14/T^{0.9}$
	Liquid	$T > T_F$
		0.01
Specific heat (J/g K)	Solid	$T > 100$ K
		3.3×10^{-4} T+0.65
	Liquid	0.42
Melting temperature (K)		$T_F = 1972$ K
Latent heat of fusion (J/g)		142
Vapor temperature (K)		3223
Latent heat of vaporization (J/g)		4715
Volumic mass (g/cm³)	Solid	2.62
	Liquid	2.32

A. MEFTAH *et al.*

istence of continuous cylindrical tracks and the electronic stopping power threshold of the chemical etching.[39] In SiO_2 quartz, this threshold lies between 4.7 and 7 keV/nm,[10] corresponding to an effective radius larger than 2 nm (Fig. 2). As the thermal spike is developed in a cylindrical geometry, the comparison between theory and experiment is limited for latent track radius larger than 2 nm.

The result of the calculations (irradiation temperature $=300$ K) is given in Fig. 7 for different values of λ and for one value of $R_d=4$ nm. This shows that the calculated radius of an equivalent molten cylinder qualitatively follows the evolution of R_e. The λ range we use is smaller than λ determined for amorphous metals and semiconductors[21] ($\lambda=19$ and 14 nm, respectively) due to the confinement of the electrons energy by the optical band gap. But the scattering of the data points compared to the calculation is due to the initial energy deposition. It can be seen from the experimental results that the same value of R_e can be reached for lower dE/dx, when the ion velocity decreases. Taking the representation in Fig. 6, the radii have been calculated for different values of D_e (Fig. 8). Then the R_e evolution versus D_e can be calculated using a unique value of λ ($\lambda=8$ nm). Using a Monte Carlo calculation, Gervais[40] has shown that the fraction of energy given up as kinematic energy to the electrons is only 0.6 to 0.8 times dE/dx. Taking such a fraction of energy it is possible to fit the experimental results by lowering λ but it is impossible to fit all the experimental R_e values if less than 60% of the dE/dx is given to the electrons.

The model does not show any significant change of the radius of the molten cylinder when the sample temperature is varied between 300 and 77 K. This is due to the fact that the energy needed to melt the material at an initial temperature of 77 K is only 5% larger than the one
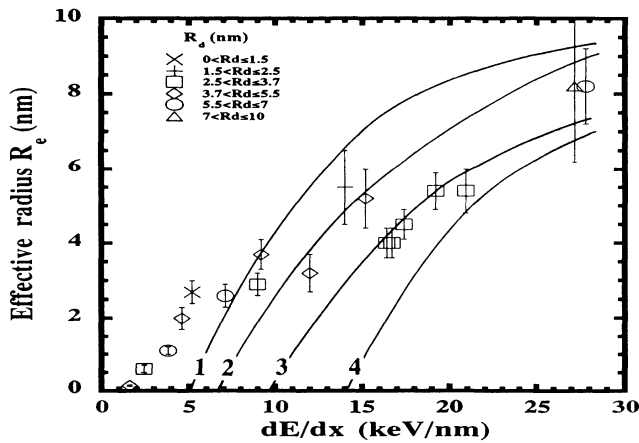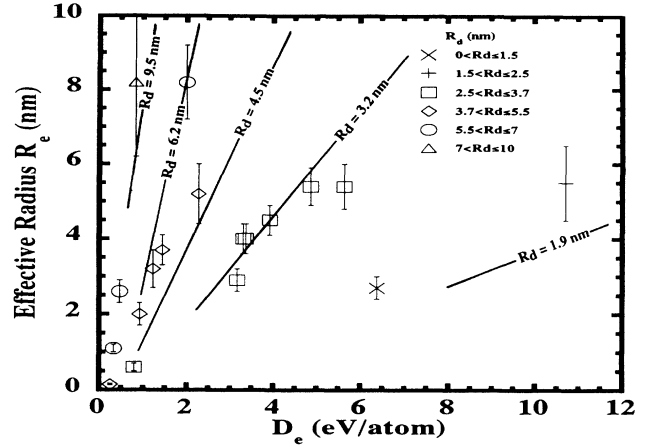

FIG. 8. The effective radius R_e vs the energy density D_e in the core of the track. The lines are fitting curves calculated from the thermal-spike model for various values of R_d and for a unique value of λ (8 nm). R_d is the radius cylinder in which 65% of dE/dx is deposited. λ is the electron mean free path of electrons. The comparison is only valid for cylindrical latent tracks (i.e., $R_e > 2$ nm).

necessary to melt a sample at 300 K. The nondependence of the damage yield on the irradiation temperature was also observed by Sigrist and Balzer.[11] They have shown that the electronic stopping power threshold for chemical etching does not change in quartz if it is irradiated at 77 K. This result of the calculation is also in agreement with the absence of any change in the damage of yttrium iron garnet and barium hexaferrite irradiated at 77 and 300 K when the latent tracks are long and cylindrical.[41] All these observations suggest that there is no significant effect of the initial value of the thermal conductivity at the irradiation temperature. This is due to the fact that the energy diffusion at the solid-liquid interface in the track core is controlled by the thermal conductivity at the melting point regardless of the temperature of irradiation. If even there was a correlation between the chemical etching and the thermal conductivity as stated by Sigrist and Balzer[11] one would have to consider the thermal conductivity at the melting point. Other materials under irradiation should be studied if we want to determine the influence of the parameters λ and/or K_e at the melting point. This would help us to understand whether the melting temperature has any influence.

VI. CONCLUSION

The cross section A of damage creation by heavy ions has been measured in SiO_2 quartz by the RBS-C technique. Using high-resolution electron microscopy, cylinders of amorphous matter have been observed whose radius is correlated to the radius of an equivalent cylinder of amorphous matter by the relation $A=\pi R_e^2$. The damage cross section can be estimated using Fig. 6, giving the energy loss and the extent R_d of the initial energy distribution. A thermal-spike model is developed in order to test whether the latent track radius can be calculated assuming that the observed amorphous phase corresponds

FIG. 7. The effective radius R_e vs the electronic stopping power dE/dx. The curves 1, 2, 3, and 4 have been calculated from the thermal spike model for $R_d=4$ nm and for various values of λ (3, 5, 8, and 11 nm, respectively). R_d is the radius of a cylinder in which 65% of dE/dx is deposited. λ is the electron mean free path of electrons. The comparison between the calculations and the experiment is only valid for $R_e > 2$ nm.

to the quench of a liquid phase. This assumption is meaningful as long as the latent tracks are continuous and cylindrical. Quantitative agreement is obtained taking into account the initial spatial energy deposition on the electrons which depends on the ion velocity. The thermal-spike model explains that no difference can be observed in the chemical etching threshold when decreasing the substrate temperature to 77 K. The good agreement between the experimental results and a description of the irradiation damage using the thermal-spike model needs now to be checked on other materials such as Al$_2$O$_3$.[42]

[1]R. L. Fleischer, P. B. Price, and R. M. Walker, *Nuclear Tracks in Solids* (University of California Press, Berkeley, 1975).

[2]D. Albretcht, P. Armbruster, R. Spohr, M. Roth, K. Schaupert, and H. Stuhmann, Appl. Phys. A **37**, 37 (1985).

[3]E. Dartyge and P. Sigmund, Phys. Rev. B **32**, 5429 (1985).

[4]F. Studer, C. Houpert, H. Pascard, R. Spohr, J. Vetter, Jim Yun Fan, and M. Toulemonde, Radiat. Eff. Def. Solids **110**, 59 (1991).

[5]A. Meftah, N. Merrien, N. Nguyen, F. Studer, H. Pascard, and M. Toulemonde, Nucl. Instrum. Methods B **59**, 605 (1991).

[6]M. Toulemonde and F. Studer, Solid State Phenomena **30**, 477 (1993).

[7]G. Bonfiglioli, A. Ferro, and A. Mojoni, J. Appl. Phys. **32**, 2499 (1961).

[8]K. Tanimura and N. Itoh, Phys. Rev. B **46**, 14 362 (1992).

[9]T. A. Tombrello, Nucl. Instrum. Methods B **2**, 555 (1984).

[10]M. Toulemonde, E. Balanzat, S. Bouffard, J. J. Grob, M. Hage-Ali, and J. P. Stoquert, Nucl. Instrum. Methods B **46**, 64 (1990).

[11]A. Sigrist and R. Balzer, Helv. Phys. Acta **50**, 49 (1977); Radiat. Eff. **34**, 75 (1977).

[12]I. A. Baranov, Yu. V. Martynenko, S. O. Tsepelevich, and Yu. N. Yavlinskii, Usp. Fiz. Nauk **156**, 477 (1988) [Sov. Phys. Usp. **31**, 1015 (1988)].

[13]R. E. Johnson, B. U. R. Sundquist, A. Hedin, and D. Fenyö, Phys. Rev. B **40**, 49 (1989).

[14]A. Dunlop, D. Lesueur, J. Morillo, J. Dural, R. Spohr, and J. Vetter, C. R. Acad. Sci. Paris **309**, 1277 (1989).

[15]A. Dunlop, P. Legrand, D. Lesueur, N. Lorenzelli, J. Morillo, A. Barbu, and S. Bouffard, Europhys. Lett. **15**, 765 (1991).

[16]C. Dufour, A. Audouard, F. Beuneu, J. Dural, J. P. Girard, A. Hairie, M. Levalois, E. Paumier, and M. Toulemonde, J. Phys: Condens. Matter **5**, 4573 (1993).

[17]A. Audouard, E. Balanzat, G. Fuchs, J. C. Jousset, D. Lesueur, and L. Thomé, Europhys. Lett. **3**, 327 (1987).

[18]S. Klaumünzer, Ming-Dong Hou, and S. Shumacher, Phys. Rev. Lett. **51**, 850 (1983).

[19]K. Izui and K. S. Furuno, in *Proceedings of the XIth International Congress on Electron Microscopy*, Kyoto, 1986, edited by T. Imura, S. Maruse, and T. Suzuki (The Japanese Society of Electron Microscopy, Tokyo, 1986), p. 1299.

[20]Ming-dong Hou, S. Klaumunzer, and S. Schumacher, Phys. Rev. B **41**, 1144 (1990).

[21]M. Toulemonde, C. Dufour, and E. Paumier, Phys. Rev. B **46**, 14 362 (1992).

[22]C. Dufour, B. Lesellier, de Chezelles, V. Delignon, M. Toulemonde, and E. Paumier, in *Modification Induced by Irradiation in Glasses*, edited by P. Mazzoldi (Elsevier Science, Amsterdam, 1992), p. 61.

[23]L. T. Chadderton and I. McTorrens, *Fission Damage in Crystals* (Methuem, London, 1969).

[24]H. Blank, Phys. Status Solidi **10**, 465 (1972).

[25]J. P. Duraud, Nucl. Instrum. Methods B **32**, 248 (1988).

[26]F. Jollet, J. P. Duraud, and C. Noguera, Radiat. Eff. Def. Solids **110**, 185 (1989).

[27]S. Bouffard, J. Dural, F. Levesque, and J. M. Ramillon, Ann. Phys. **14**, 385 (1989).

[28]J. P. Biersack and L. G. Haggmark, Nucl. Instrum. Methods **174**, 257 (1980).

[29]M. Toulemonde and F. Studer, Philos. Mag. A **58**, 799 (1988).

[30]M. R. Pascucci, J. L. Hutchison, and L. W. Hobbs, Radiat. Eff. **74**, 219 (1983).

[31]A. Meftah, F. Brisard, J. M. Costantini, M. Hage-Ali, J. P. Stoquert, F. Studer, and M. Toulemonde, Phys. Rev. B **48**, 920 (1993).

[32]R. Katz and E. J. Kobetich, Phys. Rev. **186**, 344 (1969).

[33]M. P. R. Waligorski, R. N. Hamm, and R. Katz, Nucl. Tracks Radiat. Meas. **11**, 309 (1986).

[34]I. M. Lifshits, M. I. Kaganov, and L. V. Tanatarov, J. Nucl. Energy A **12**, 69 (1960).

[35]Yu. V. Martynenko and Yu. N. Yavlinski, Dokl. Akad. Nauk (SSSR) **270**, 88 (1983) [Sov. Phys. Dokl. **28**, 391 (1983)].

[36]F. Seitz and J. S. Koelher, Solid State Phys. **2**, 305 (1956).

[37]M. Toulemonde, G. Fuchs, N. Nguyen, F. Studer, and D. Groult, Phys. Rev. B **35**, 6560 (1987).

[38]A. Meftah, M. Hage-Ali, J. P. Stoquert, F. Studer, and M. Toulemonde, Radiat. Eff. Def. Solids **126**, 251 (1993).

[39]M. Toulemonde, N. Enault, Jin Yun Fan, and F. Studer, J. Appl. Phys. **4**, 68 (1990).

[40]B. Gervais, Ph.D. thesis, University of Caen, 1993.

[41]C. Houpert, F. Studer, H. Pascard, Jin Yun Fan, and M. Toulemonde, Nucl. Tracks Radiat. Meas. **19**, 185 (1991).

[42]B. Canut, S. M. M. Ramos, P. Thevenard, N. Moncoffre, A. Benyagoub, G. Marest, A. Meftah, F. Studer, and M. Toulemonde, Nucl. Instrum. Methods B **80/81**, 1114 (1993).
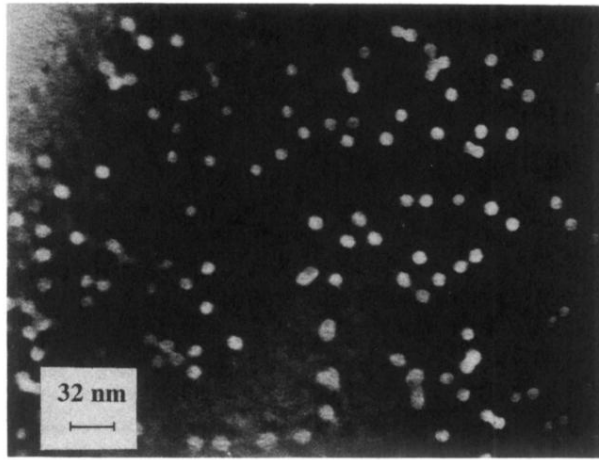
FIG. 3. Medium resolution electron microscopy observation of SiO_2 quartz irradiated by Pb ions ($E = 0.3$ MeV/amu; $\phi t = 1.4 \times 10^{11}$ ions/cm^2).
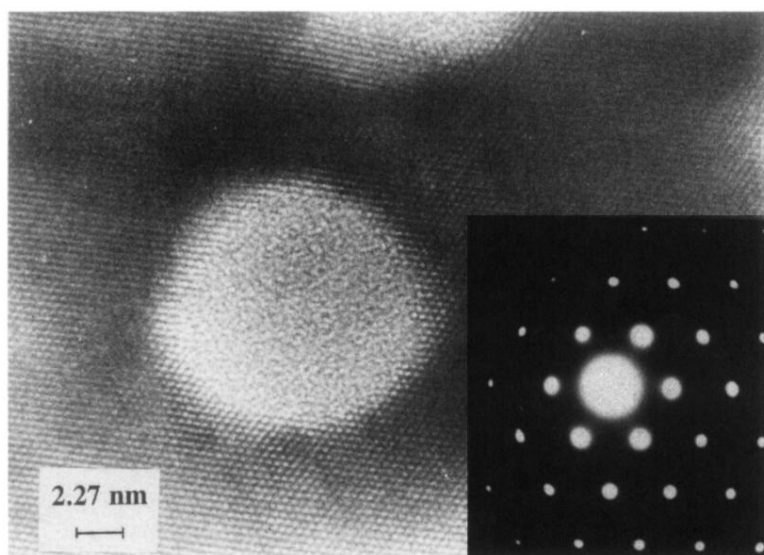
FIG. 4. High-resolution electron micrograph of an amorphized fragment of SiO_2 irradiated by Pb ions (0.3 MeV/amu). The electron diffraction in the inset shows typical diffuse rings indicating the presence of the amorphous phase.